Ponnapalli, Bradley, Devine, Bowen, Coppens, Leraas, Milash, Li, Luo, Qiu, Wu, Yang, Wittwer, Palmer, Jensen, Gastier-Foster, Hanson, Barnholtz-Sloan & Alter (2020)

Retrospective clinical trial experimentally validates glioblastoma genome-wide pattern of DNA copy-number alterations predictor of survival

Supplementary Methods, Figs. S1–S12, and Tables S1–S4

Clinical patient information and tumor sample acquisition. Patients were retrospectively enrolled at the Case Western Reserve University (CWRU) tissue source site that had received no treatment for glioblastoma (GBM) prior to the surgery, and had at least one frozen tumor sample that weighed ≥100 mg available in the biobank. A frozen section slide was cut from each sample and haematoxylin-and-eosin stained, and the diagnosis of GBM was confirmed by a neuropathologist.

DNA extraction. The tumor samples were shipped to the Nationwide Children's Hospital (NCH) biospecimen core resource in cryoports that maintained an average temperature of ≤−180℃. A portion of ≈40 mg was cut from each sample that weighed ≥90 mg. A slide was cut from each portion, stained, and digitally imaged (Leica® Biosystems, Aperio™). The diagnosis was reconfirmed and the slide percent tumor nuclei and necrosis were estimated by a neuropathologist. If there were <60% tumor nuclei or >50% necrosis, the portion was excluded. If there remained ≥40 mg from the corresponding sample, an additional portion was cut, and if not, the sample was excluded.

An analyte DNA sample was purified from the remaining part of each tumor portion that passed the quality controls (QIAGEN®, AllPrep® DNA/RNA) and was tested for minimal degradation by using gel electrophoresis. The concentration (Thermo Fisher Scientific®, PicoGreen®) and volume of each sample were measured. This resulted in 120 analyte DNA samples, >3 µg each, from the tumors of 120 patients. At least two aliquot DNA samples of ≥1.5 µg each were prepared from each analyte DNA sample. The two sets were shipped in cryoports, one to a genomic characterization center of the Cancer Genome Atlas (TCGA), viz., the Broad Institute (BI), and the other to the Beijing Genomics Institute (BGI) -Shenzhen.

Whole-genome sequencing. At BI, the concentration (Thermo Fisher Scientific®, PicoGreen®) and volume of each aliquot DNA sample were measured, and aliquots of <1 µg were replaced by others from the same analyte DNA samples. A 350-ng part of each aliquot was sheared to 385-base pair fragments (Covaris®, E220™) and converted into a sequencing library. Up to 24 libraries were sequenced at a time, one library per flow cell lane, to obtain 151-nucleotide paired-end sequence reads (Illumina®, HiSeq X®). If the genomic coverage was estimated to be below the 30X target and there was material remaining from the library, it was additionally sequenced, but if a new library was needed, it was constructed from an additional 350-ng part of the aliquot and sequenced. The raw data from the different sequencing runs of the different libraries of the same aliquot DNA sample were aggregated, mapped to hg38, and converted to a compressed alignment map (CRAM) file (BI, Picard©). To control for the aliquot DNA source of each CRAM file, a part of each aliquot DNA sample was fingerprinted by a 96-single-nucleotide polymorphism (SNP) assay and compared with the sequence data in the CRAM file. This polymerase chain reaction (PCR) amplification-free whole genome sequencing (WGS) resulted in 120 CRAM files of the tumors of the 120 patients.

At BGI-Shenzhen, each aliquot DNA sample was tested for minimal degradation by using gel electrophoresis, and its concentration (Thermo Fisher Scientific®, Qubit®) and volume were measured. Aliquots of <1.5 µg were excluded. A 1.5-µg part of each remaining aliquot was sheared to ≈280-base pair fragments (Covaris®, E220™) and converted into single-stranded DNA (ssDNA) circles. Aliquots that yielded <12 ng ssDNA circles each were excluded. The ssDNA circles were rolling circle-replicated in tandem into ssDNA coils, i.e., DNA nanoballs (DNBs). Aliquots that yielded <6 ng DNBs were excluded. The DNBs were adsorbed onto patterned arrays and sequenced to obtain 100-nucleotide paired-end reads providing an estimated ≥30X coverage (BGI, BGISEQ-500). The raw data from each aliquot DNA sample were mapped to hg19 after removing reads containing adapter sequences, converted to a binary alignment map (BAM) file, and mapped to a message digest 5 (MD5) hash code (BGI, SOAPnuke©). BAM files that failed the MD5 checksum were excluded. This PCR-free WGS resulted in 104 BAM files of the tumors of 104 of the 120 patients.

BAM and CRAM file preprocessing. Of the 212,696 Agilent comparative genomic hybridization (CGH) probes that define the GBM pattern across the autosome and the X chromosome, which are of unique sequences and hg18 coordinates, 212,494 were mapped to unique hg19 coordinates (University of California at Santa Cruz, UCSC Genome Browser©). Of the same

212,696 probes, 212,348 were mapped to unique hg38 coordinates (A. Dobin, STAR Aligner©). The mapping to hg38 was tested for negligible discrepancy with the mapping to hg19. Each 45- to 60-nucleotide probe was converted to a genomic bin that extends from 500 nucleotides before to 500 nucleotides after the start and end coordinates of the probe, respectively. The number of reads that map to each bin in hg19 and, separately, hg38 was counted in each raw CRAM and BAM file, respectively (Sanger Institute, SAMtools©). Read counts of zero were nulled. This resulted in 120 hg38 and 104 hg19 minimally preprocessed profiles from the tumors of the 120 and the 104 of the 120 patients, respectively.

To control for the analyte DNA sources of the CRAM and BAM files, Pearson correlations were computed between the hg38 and hg19 profiles of the 104 patients across the subset of 211,653 bins, which, at >99.5% of either the hg38 or hg19 probe sets, maintain the same chromosomal order in both reference human genomes. Each hg38 profile was paired with the one hg19 profile of the 104, which it is most correlated with. Similarly, each hg19 profile was paired with the one hg38 profile of the 104, which it is most correlated with. The hg38 and hg19 profiles of seven of the 104 patients failed to pair with each other, and the seven patients were excluded. The 16 patients with only CRAM files but no BAM files, which could not be tested, were excluded as well.

Note that as in the previous modeling of genomic profiles from TCGA, the classifications of the Utah profiles were constant under, i.e., robust to, changes in the preprocessing of the profiles. The changes included, e.g., skipping reads that were flagged as technical duplicates or quality control failures, reducing the bin sizes by two orders of magnitude to the Agilent probe sizes, and removing probes to accommodate one-to-one mapping to nonoverlapping hg19 and, separately, hg38 bins of sizes in the range of 500 to 1,500 nucleotides (G. Klambauer, cn.MOPS©).

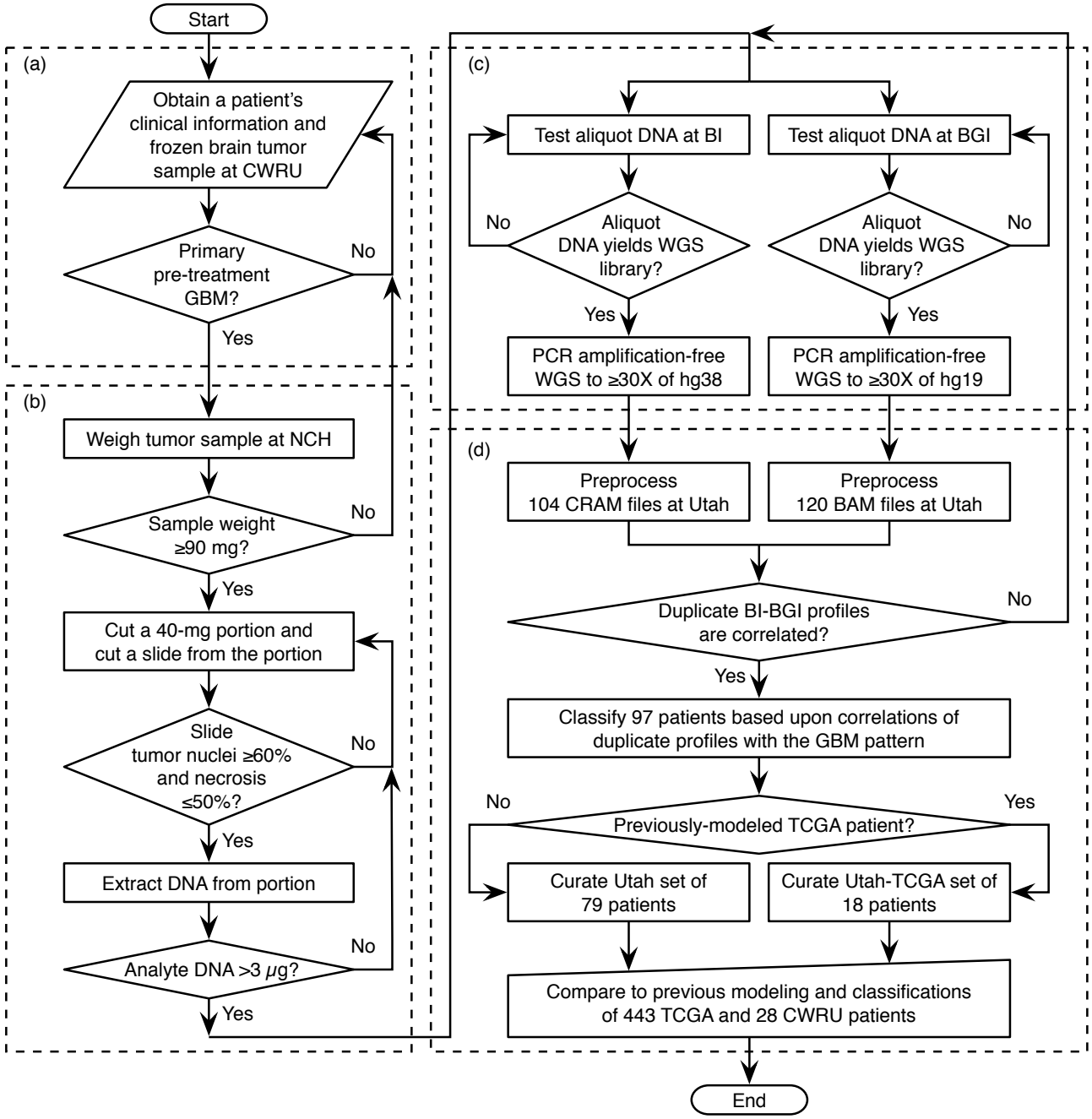

Fig. S1. The experimental workflow was similar to that of TCGA and the computational workflow was similar to that previously used to establish and (re)validate the GBM pattern in the sets of GBM and lower-grade astrocytoma (LGA) patients from TCGA. (*a*) Clinical patient information and tumor sample acquisition at the CWRU tissue source site. (*b*) DNA extraction at the NCH biospecimen core resource. (*c*) WGS at a TCGA genomic characterization center, viz., BI, and BGI. (*d*) Classification of the tumor profiles by correlation with the GBM pattern and comparison to the previous modeling and classifications of TCGA profiles at Utah.

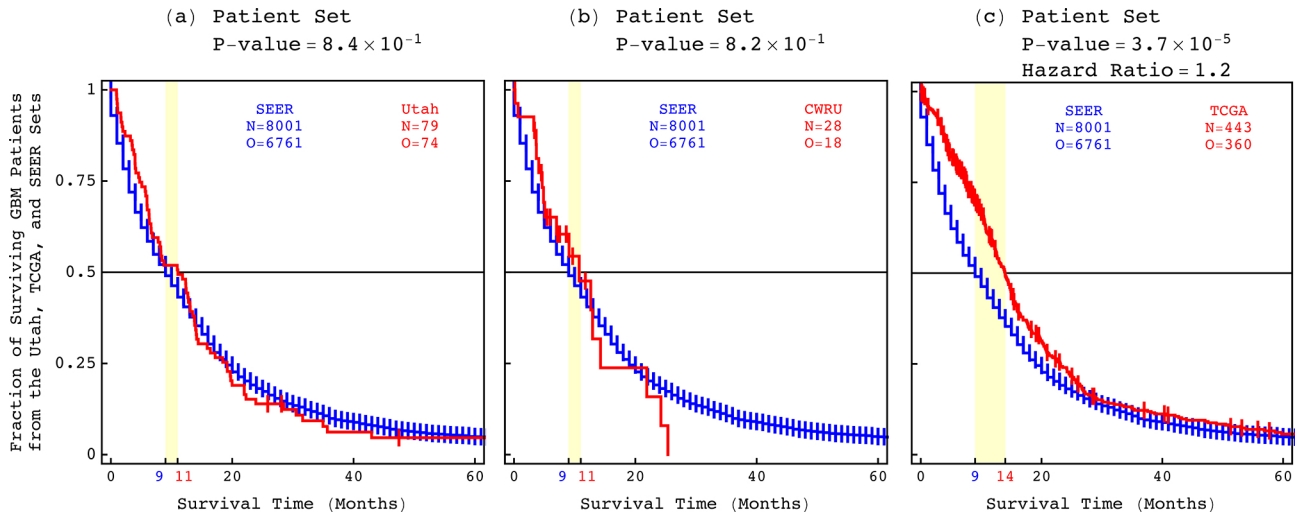

Fig. S2. The Utah set of 79 patients statistically represents the U.S. adult GBM population in terms of the disease phenotype of median survival. In Kaplan-Meier (KM) survival analyses, the approximately nine-month median survival of the 8,001 Surveillance, Epidemiology, and End Results (SEER) patients is statistically indistinguishable from the 11-month median survival times of the (*a*) 79 Utah and (*b*) 28 CWRU patients, with the corresponding log-rank *P*-values >0.05. (*c*) The nine-month median survival of the SEER patients, however, is statistically significantly shorter than the 14 months of the 443 TCGA patients.

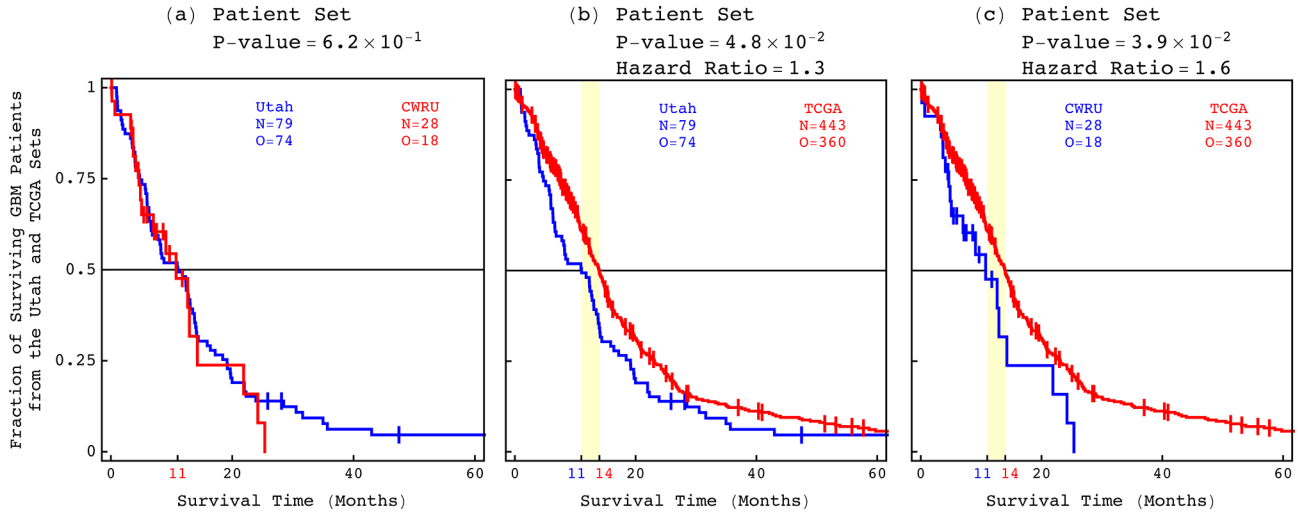

Fig. S3. The Utah set of 79 patients statistically represents the surgical case series of CWRU in terms of the disease phenotype of median survival. (*a*) The approximately 11-month median survival of the 79 Utah patients is statistically indistinguishable from that of the 28 CWRU patients, with the corresponding log-rank *P*-value >0.05. The 11-month median survival times of the (*b*) Utah and (*c*) CWRU patients, however, are statistically significantly shorter than the 14 months of the 443 TCGA patients.

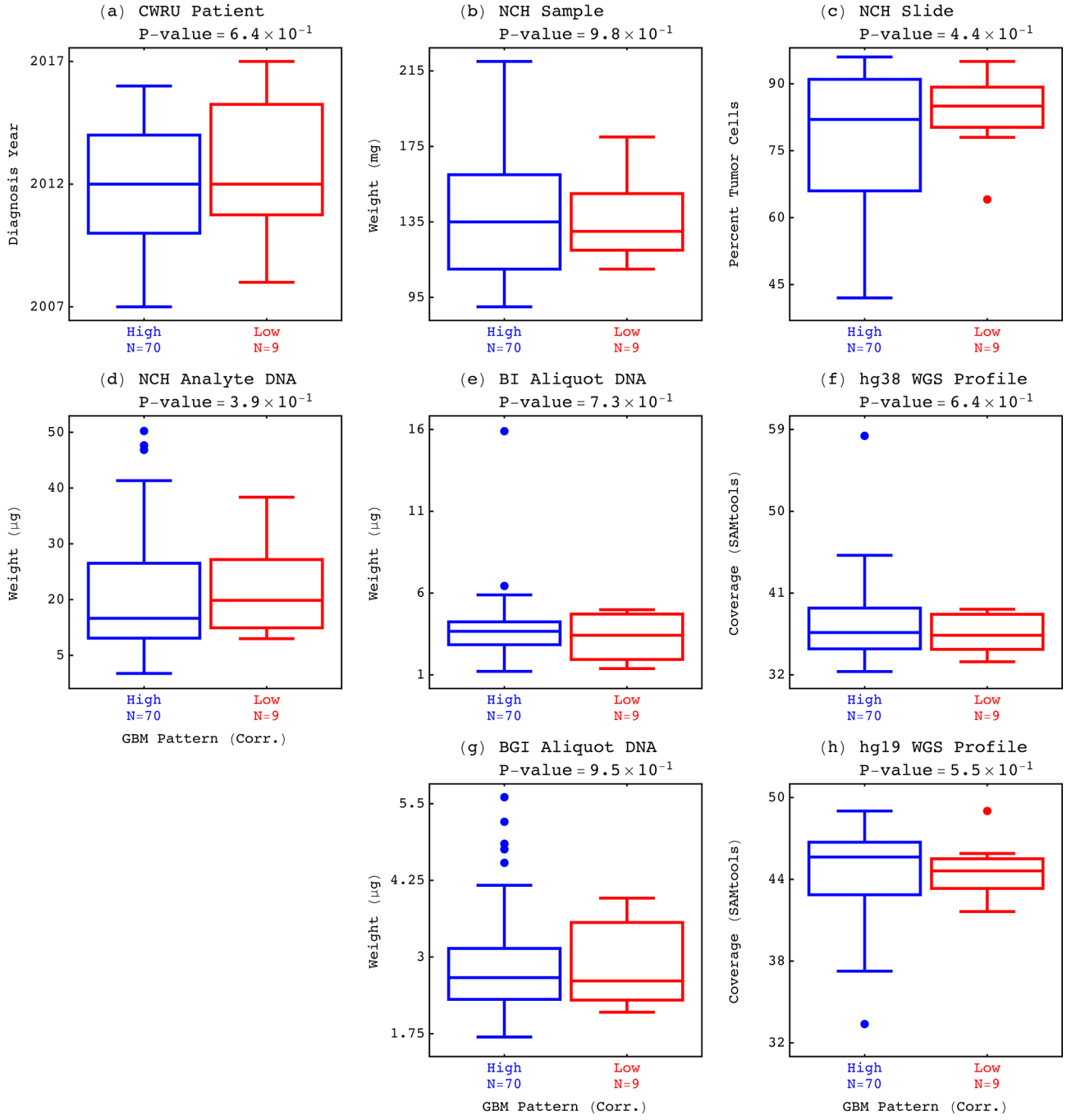

Fig. S4. Experimental, biological, and clinical parameters other than survival are statistically indistinguishable in the classification of the Utah set of 79 patients by the GBM pattern, with the corresponding Mann-Whitney-Wilcoxon (MWW) *P*-values >0.05.

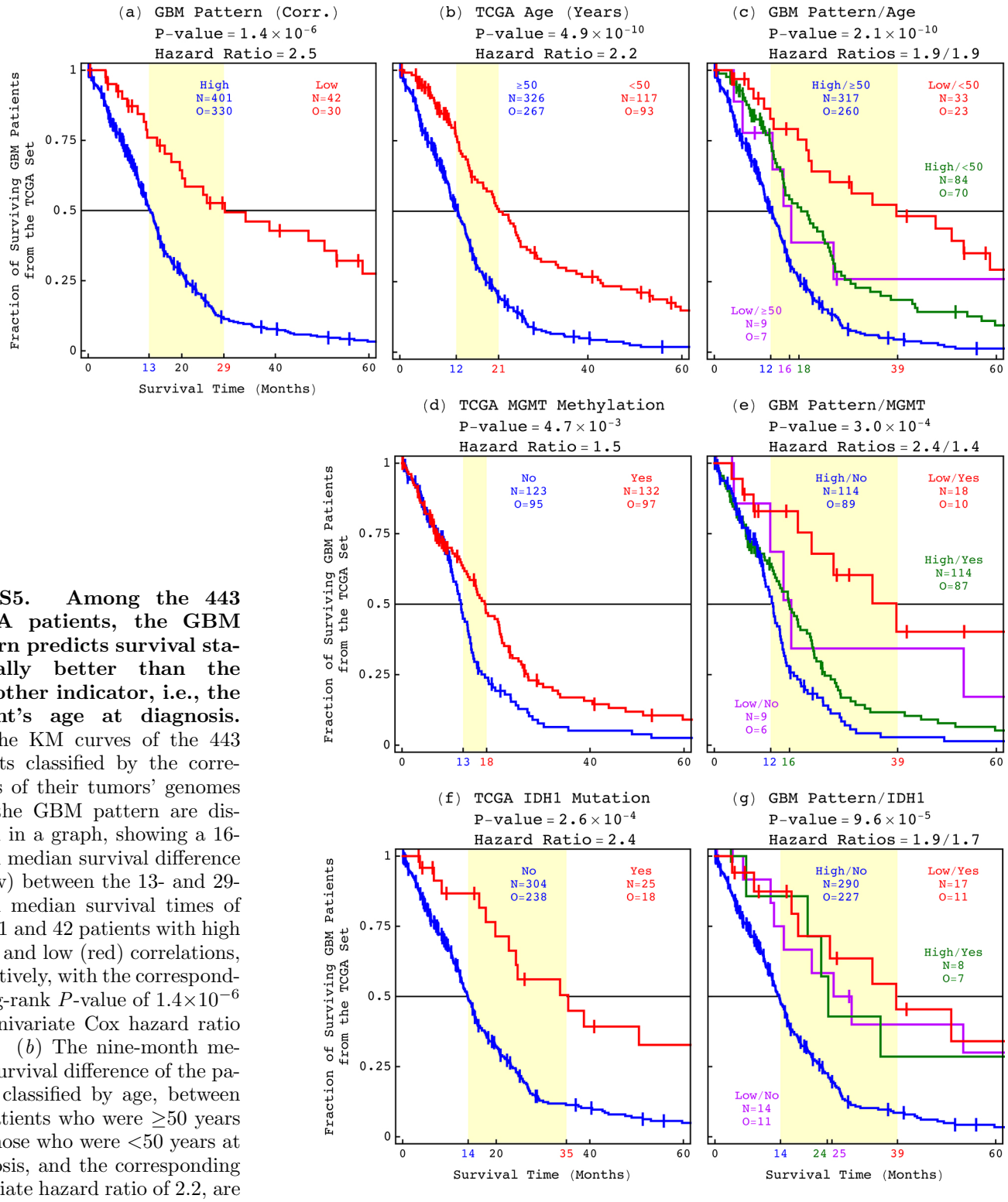

Fig. S5. Among the 443 TCGA patients, the GBM pattern predicts survival statistically better than the best other indicator, i.e., the patient's age at diagnosis. (*a*) The KM curves of the 443 patients classified by the correlations of their tumors' genomes with the GBM pattern are displayed in a graph, showing a 16-month median survival difference (yellow) between the 13- and 29-month median survival times of the 401 and 42 patients with high (blue) and low (red) correlations, respectively, with the corresponding log-rank *P*-value of 1.4×10^{-6} and univariate Cox hazard ratio of 2.5. (*b*) The nine-month median survival difference of the patients classified by age, between the patients who were $\geq$50 years and those who were <50 years at diagnosis, and the corresponding univariate hazard ratio of 2.2, are less than those of the patients classified by the pattern. (*c*) The 21-month median survival difference of the 117 patients who were <50 years at diagnosis, and are classified by the pattern into 84 and 33 patients who in addition were with high and low correlations, respectively, is greater than the nine-month median survival of the classification of the 443 patients by age alone. (*d*) The median survival of the 132 patients with a methylated O^6-methylguanine-DNA methyltransferase (*MGMT*) promoter is 18 months. (*e*) A low correlation with the pattern identifies 18 patients of a 39-month median survival among the 132 patients with a methylated *MGMT* promoter. (*f*) The median survival of the 25 patients with a mutated isocitrate dehydrogenase 1 (*IDH1*) is 35 months. (*g*) A low correlation identifies 17 patients of a 39-month median survival among the 25 patients with a mutated *IDH1*.

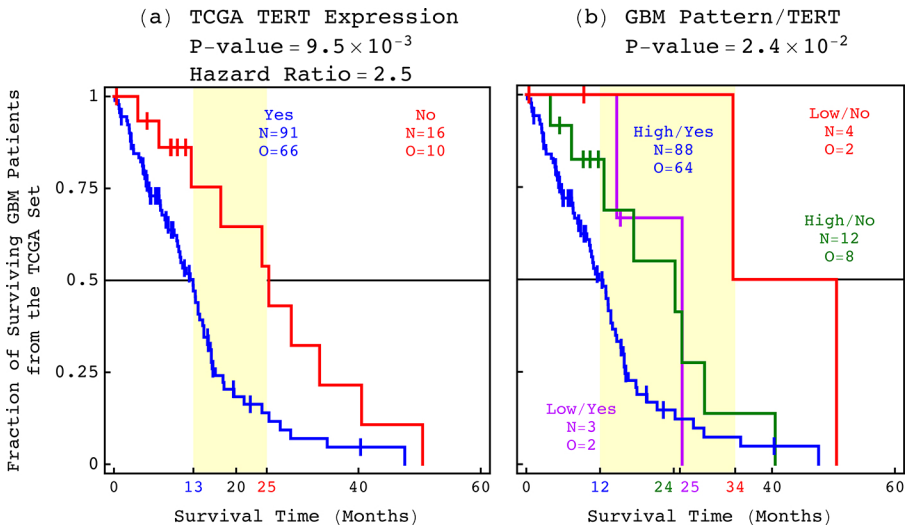

Fig. S6. Among the TCGA patients, the GBM pattern predicts survival better than telomerase reverse transcriptase (*TERT*) gene expression, the most recent indicator of survival to have advanced to standard of care. (*a*) The median survival of the 16 patients with no *TERT* expression is 25 months. (*b*) A low correlation with the pattern identifies four patients of a 34-month median survival among the 16 patients.

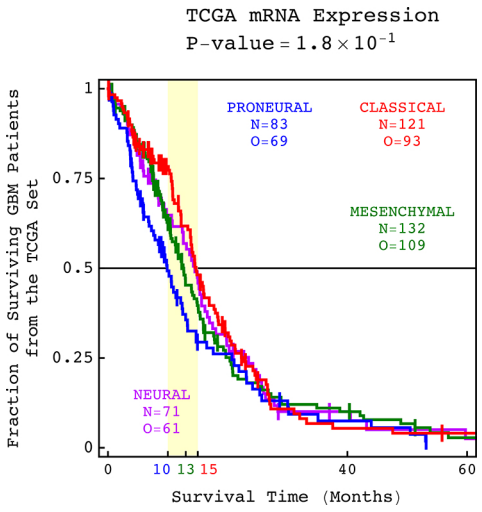

Fig. S7. Subtypes based upon mRNA expression of a few hundred genes do not indicate GBM survival. The median survival times of the 407 TCGA patients with a proneural, mesenchymal, classical, or neural subtype designation, e.g., when classified into these subtypes, are statistically indistinguishable, with the corresponding log-rank *P*-value >0.05.

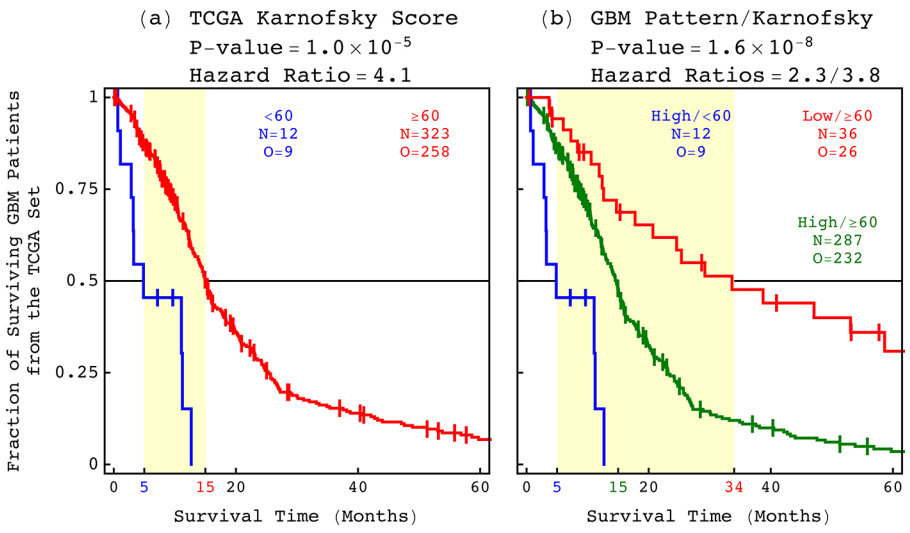

Fig. S8. Among the TCGA patients, the GBM pattern is a predictor of survival independent of the Karnofsky performance score. (*a*) The median survival of the 323 patients with a Karnofsky score ≥60 is 15 months. (*b*) A low correlation with the pattern identifies 36 patients of a 34-month median survival among the 323 patients.

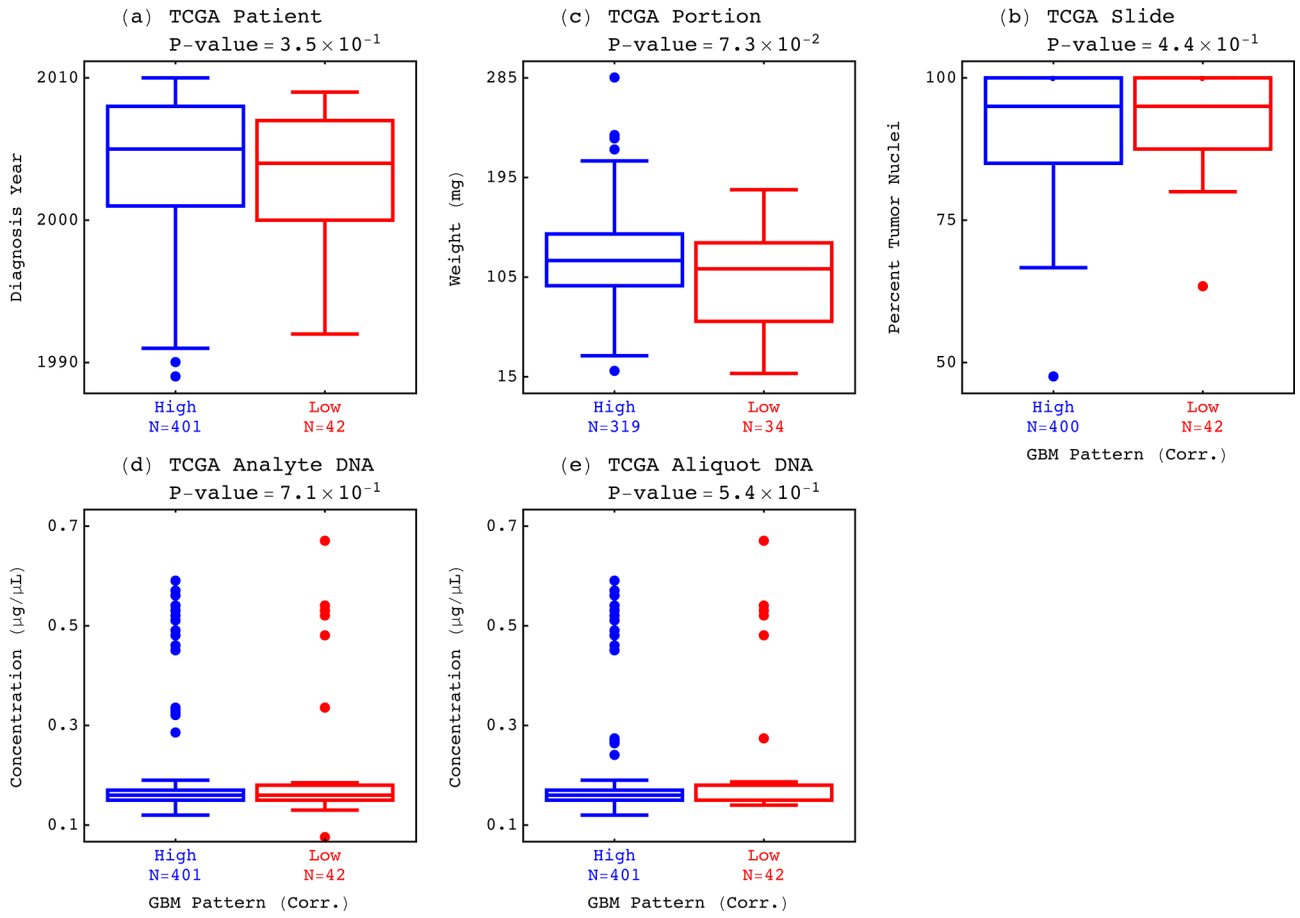

Fig. S9. Experimental, biological, and clinical parameters other than survival are statistically indistinguishable in the classification of the TCGA set of 443 patients by the GBM pattern, with the corresponding MWW *P*-values >0.05.

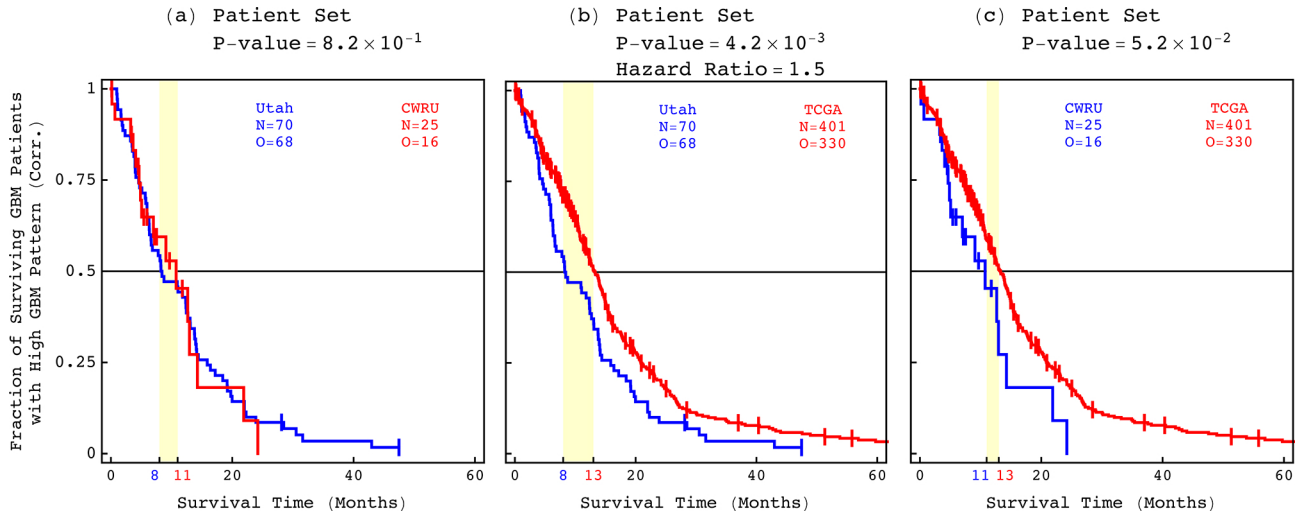

Fig. S10. The CWRU surgical case series statistically represents the Utah set of 79 patients in terms of the disease phenotype of median survival conferred by a high correlation with the GBM pattern. (*a*) The eight-month median survival of the 70 of the 79 Utah patients with high correlations with the pattern is statistically indistinguishable from the 11-month, i.e., roughly one-year of the 25 of the 28 CWRU patients, (*b*) but shorter than the 13 months of the 401 of the 443 TCGA patients. (*c*) The 11-month median survival of the CWRU patients, however, is statistically indistinguishable from the 13 months of the TCGA patients.

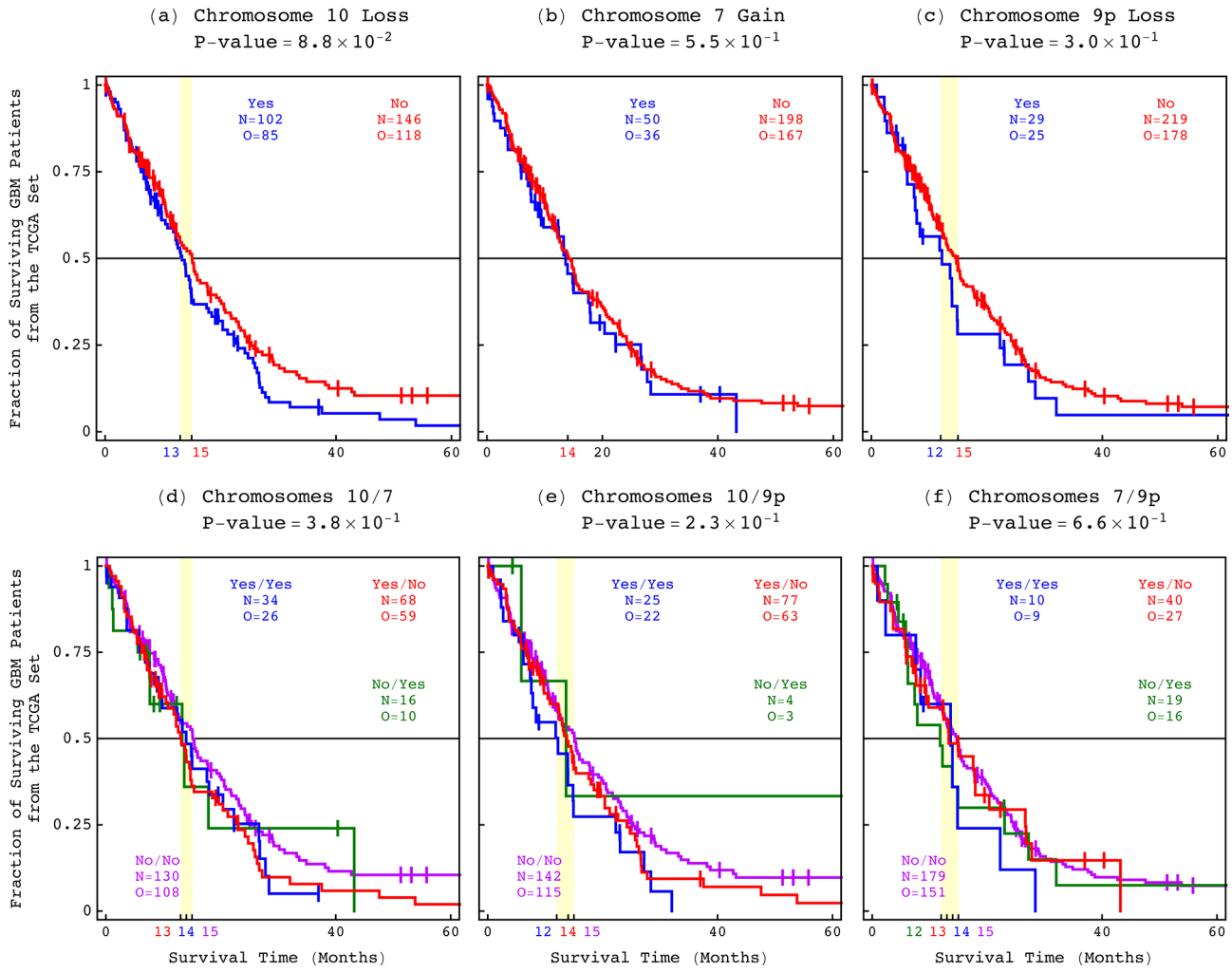

Fig. S11. Frequently observed in GBM tumors and notable in the GBM pattern, neither one nor any combination of chromosome 10 deletion, chromosome 7 amplification, and chromosome arm 9p deletion, indicates survival. The median survival times of the 248 TCGA patients with chromosome number change classifications, e.g., are statistically indistinguishable, with the corresponding log-rank *P*-values >0.05.

Fig. S12. Among the TCGA patients, amplifications of two of the 130 segments identified in the GBM pattern, one with the transfer RNA (tRNA) methyltransferase-like 2B (*METTL2B*), the other with its homolog methyltransferase-like 2A (*METTL2A*) and the nuclear localization sequence-encoding part of the serine/threonine tousled-like kinase 2 (*TLK2*) indicate survival. That these putative drug targets and combinations of targets are correlated with survival may lead to new agents for GBM treatment.

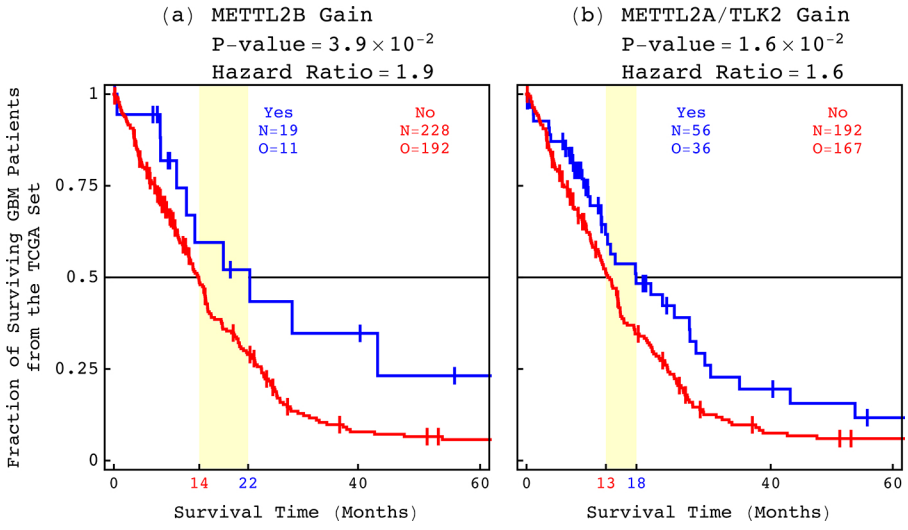

Phenotype		Group	Utah Set	CWRU Set	TCGA Set	SEER Set	Utah vs. SEER χ^2 P-Value	CWRU vs. SEER χ^2 P-Value	TCGA vs. SEER χ^2 P-Value
Normal	Sex	Female	27	12	169	3331	1.8×10^{-1}	9.0×10^{-1}	1.5×10^{-1}
		Male	52	16	274	4670			
	Race	Not White	5	3	40	959	1.2×10^{-1}	8.4×10^{-1}	1.1×10^{-1}
		White	74	25	386	7042			
	Ethnicity	Hispanic	2	0	11	507	1.7×10^{-1}	1.7×10^{-1}	4.4×10^{-3}
		Not Hispanic	77	28	382	7494			
Disease	Age (Years)	<50	10	3	117	1164	6.4×10^{-1}	5.7×10^{-1}	1.2×10^{-11}
		≥50	69	25	326	6837			

Table S1. The Utah set of 79 patients statistically represents the U.S. adult GBM population in terms of the disease phenotype of age at diagnosis. The distributions of the disease phenotype of age at diagnosis and the normal phenotypes of sex, race, and ethnicity of the SEER patients are statistically indistinguishable from the distributions of the Utah and CWRU patients, with the corresponding χ^2 P-values >0.05. The distribution of the disease phenotype of age at diagnosis of the SEER patients is statistically significantly different from the distribution of the TCGA patients, with the corresponding χ^2 P-value of 1.2×10^{-11}.

Patients (Number)	Predictor	KM Group	Median (Months)	Log-Rank P-Value	Cox Model	Hazard Ratio	95% Confidence Interval	Wald P-Value	Concordance Index
79	GBM Pattern (Corr.)	Low	35	2.5×10^{-3}	Univariate	3.5	1.5– 8.2	4.3×10^{-3}	0.78
		High	8						
	CWRU Age (Years)	<50	19	3.7×10^{-3}		3.3	1.4– 7.5	6.1×10^{-3}	0.78
		≥50	8						
	GBM Pattern (Corr.)	Low/<50		5.2×10^{-3}	Bivariate	2.6	1.1– 6.3	3.4×10^{-2}	0.76
	CWRU Age (Years)	Low/≥50	20			2.4	1.0– 5.7	5.0×10^{-2}	
		High/<50	14						
		High/≥50	8						
47	GBM Pattern (Corr.)	Low	36	4.8×10^{-3}	Univariate	4.1	1.4– 11.8	8.7×10^{-3}	0.86
		High	14						
	CWRU Age (Years)	<50	28	7.9×10^{-3}		3.7	1.3– 10.5	1.3×10^{-2}	0.81
		≥50	14						
59	GBM Pattern (Corr.)	Low	36	2.0×10^{-3}		4.6	1.6– 13.0	4.3×10^{-3}	0.88
		High	12						
	CWRU Age (Years)	<50	19	1.7×10^{-2}		2.7	1.2– 6.4	2.2×10^{-2}	0.72
		≥50	13						
75	GBM Pattern (Corr.)	Low	35	2.1×10^{-3}		4.0	1.6– 10.1	4.0×10^{-3}	0.79
		High	8						
	CWRU Chemotherapy	Yes	14	1.0×10^{-12}		6.0	3.5– 10.4	7.0×10^{-11}	0.93
		No	4						
	CWRU Radiation	Yes	13	4.4×10^{-15}		10.8	5.3– 22.1	7.6×10^{-11}	0.93
		No	2						
74/75	GBM Pattern (Corr.)	Low/Yes	36	1.5×10^{-12}	Bivariate	3.8	1.3– 10.8	1.4×10^{-2}	0.91
	CWRU Chemotherapy	High/Yes	14			5.0	2.9– 8.6	9.0×10^{-9}	
		High/No	4						
	GBM Pattern (Corr.)	Low/Yes	36	4.2×10^{-15}		4.6	1.6– 13.0	4.4×10^{-3}	0.92
	CWRU Radiation	High/Yes	12			9.3	4.5– 19.3	1.6×10^{-9}	
		High/No	3						
52	GBM Pattern (Corr.)	Low	35	8.1×10^{-3}	Univariate	3.2	1.3– 7.9	1.1×10^{-2}	0.74
		High	12						
	CWRU Karnofsky Score	≥60	16	7.3×10^{-7}		5.8	2.7– 12.4	8.0×10^{-6}	0.87
		<60	5						
51/52	GBM Pattern (Corr.)	Low/≥60	35	1.3×10^{-6}	Bivariate	3.5	1.3– 9.4	1.3×10^{-2}	0.83
	CWRU Karnofsky Score	High/≥60	14			4.5	2.0– 9.9	2.0×10^{-4}	
		High/<60	5						
28	GBM Pattern (Corr.)	Low	35	6.1×10^{-3}	Univariate	10.6	1.4– 80.9	2.3×10^{-2}	0.97
		High	6						
	CWRU Percent Resection	≥30	12	3.0×10^{-2}		2.8	1.1– 7.6	3.9×10^{-2}	0.73
		<30	5						
	GBM Pattern (Corr.)	Low/≥30	35	4.5×10^{-3}	Bivariate	9.8	1.3– 76.2	2.9×10^{-2}	0.80
	CWRU Percent Resection	High/≥30	8						
		High/<30	5						

Table S2. Among the 79 Utah patients, the GBM pattern is a predictor of survival independent of age and the treatments, i.e., chemotherapy and radiation. The bivariate hazard ratios of the classifications by the pattern and age, chemotherapy, radiation, or the Karnofsky score are consistently within the 95% confidence intervals of the corresponding univariate ratios. The univariate ratio of the classification by the pattern is within the 95% confidence interval of the corresponding bivariate ratio of the classification by both the pattern and percent resection. The concordance indices, i.e., accuracies, of the classifications by the pattern are consistently greater than or the same as those by age. This is among the 79 patients, the 47 chemotherapy- and 59 radiation-treated patients, the 75 patients with treatment information and the 74 patients among them excluding the one untreated patient whose tumor profiles have low correlations with the GBM pattern, the 52 patients with Karnofsky score information and the 51 patients among them excluding the one patient whose tumor profiles have low correlations with the GBM pattern and whose Karnofsky score is <60, and the 28 patients with percent resection information.

Phenotype		Group	Utah Set	CWRU Set	TCGA Set	Utah vs. CWRU χ^2 P-Value	Utah vs. TCGA χ^2 P-Value	CWRU vs. TCGA χ^2 P-Value
Disease	GBM Pattern (Corr.)	Low	9	3	42	9.2×10^{-1}	6.0×10^{-1}	8.3×10^{-1}
		High	70	25	401			
	MGMT Methylation	Yes	3	16	132	2.3×10^{-1}	4.3×10^{-1}	3.4×10^{-1}
		No	5	10	123			
	IDH1 Mutation	Yes	5	2	25	8.7×10^{-1}	4.4×10^{-1}	7.5×10^{-1}
		No	41	19	304			
	Karnofsky Score	<60	11	4	12	9.9×10^{-1}	6.2×10^{-7}	3.6×10^{-4}
		≥60	41	15	323			

Table S3. The TCGA patients statistically represent the Utah set of 79 patients in terms of the disease phenotypes of *MGMT* promoter methylation, *IDH1* mutation, and the GBM pattern. The distributions of the disease phenotypes of *MGMT*, *IDH1*, and the GBM pattern of the Utah patients are statistically indistinguishable from the distributions of the TCGA and CWRU patients, with the corresponding χ^2 P-values >0.05.

Table S4 (on p. S13). Among the 443 TCGA patients, the GBM pattern is a predictor of survival better than and independent of the existing pathology laboratory tests, i.e., for *MGMT* promoter methylation and *IDH1* mutation, as well as better than *TERT* gene expression. The bivariate hazard ratios of the classifications by the pattern and age, *MGMT*, or *IDH1* are consistently within the 95% confidence intervals of the corresponding univariate ratios. Similarly, the concordance indices, i.e., accuracies, of the classifications by the pattern are consistently greater than those by age. This is among the 443 patients, the 284 chemotherapy- and 327 radiation-treated patients, the 255 *MGMT*- and 329 *IDH1*-tested patients, the 107 *TERT*-classified patients, and the 335 patients with Karnofsky score information.

Patients (Number)	Predictor	KM Group	Median (Months)	Log-Rank *P*-Value	Cox Model	Hazard Ratio	95% Confidence Interval	Wald *P*-Value	Concordance Index
443	GBM Pattern (Corr.)	Low	29	1.4×10^{-6}	Univariate	2.5	1.7– 3.6	2.9×10^{-6}	0.75
		High	13						
	TCGA Age (Years)	<50	21	4.9×10^{-10}		2.2	1.7– 2.8	1.1×10^{-9}	0.72
		≥50	12						
	GBM Pattern (Corr.)	Low/<50	39	2.1×10^{-10}	Bivariate	1.9	1.3– 2.8	1.7×10^{-3}	0.71
	TCGA Age (Years)	High/<50	18			1.9	1.4– 2.4	1.9×10^{-6}	
		Low/≥50	16						
		High/≥50	12						
284	GBM Pattern (Corr.)	Low	50	3.2×10^{-4}	Univariate	2.5	1.5– 4.1	4.9×10^{-4}	0.73
		High	15						
	TCGA Age (Years)	<50	22	3.3×10^{-5}		1.9	1.4– 2.6	4.3×10^{-5}	0.64
		≥50	15						
	GBM Pattern (Corr.)	Low/<50	50	5.5×10^{-5}	Bivariate	1.8	1.1– 3.2	2.9×10^{-2}	0.64
	TCGA Age (Years)	High/<50	18			1.6	1.1– 2.2	6.8×10^{-3}	
		High/≥50	15						
		Low/≥50	6						
327	GBM Pattern (Corr.)	Low	39	2.8×10^{-5}	Univariate	2.4	1.6– 3.8	4.8×10^{-5}	0.73
		High	15						
	TCGA Age (Years)	<50	23	6.7×10^{-6}		1.9	1.4– 2.5	8.9×10^{-6}	0.66
		≥50	15						
	GBM Pattern (Corr.)	Low/<50	47	2.7×10^{-6}	Bivariate	2.0	1.3– 3.1	3.0×10^{-3}	0.65
	TCGA Age (Years)	High/<50	20			1.6	1.2– 2.1	1.7×10^{-3}	
		Low/≥50	16						
		High/≥50	15						
255	GBM Pattern (Corr.)	Low	34	3.2×10^{-4}	Univariate	2.5	1.5– 4.2	5.0×10^{-4}	0.73
		High	13						
	TCGA *MGMT* Methylation	Yes	18	4.7×10^{-3}		1.5	1.1– 2.0	5.0×10^{-3}	0.58
		No	13						
	GBM Pattern (Corr.)	Low/Yes	39	3.0×10^{-4}	Bivariate	2.4	1.4– 4.0	1.1×10^{-3}	0.61
	TCGA *MGMT* Methylation	Low/No	16			1.4	1.1– 1.9	1.7×10^{-2}	
		High/Yes	16						
		High/No	12						
329	GBM Pattern (Corr.)	Low	34	5.5×10^{-5}	Univariate	2.4	1.6– 3.8	9.2×10^{-5}	0.77
		High	14						
	TCGA *IDH1* Mutation	Yes	35	2.6×10^{-4}		2.4	1.5– 3.9	4.0×10^{-4}	0.78
		No	14						
	GBM Pattern (Corr.)	Low/Yes	39	9.6×10^{-5}	Bivariate	1.9	1.2– 3.1	8.4×10^{-3}	0.77
	TCGA *IDH1* Mutation	Low/No	25			1.7	1.0– 3.0	4.1×10^{-2}	
		High/Yes	24						
		High/No	14						
107	GBM Pattern (Corr.)	Low	34	1.8×10^{-2}	Univariate	3.7	1.2– 12.1	2.7×10^{-2}	0.90
		High	13						
	TCGA *TERT* Expression	No	25	9.5×10^{-3}		2.5	1.2– 5.1	1.2×10^{-2}	0.77
		Yes	13						
	GBM Pattern (Corr.)	Low/No	34	2.4×10^{-2}	Bivariate				0.80
	TCGA *TERT* Expression	Low/Yes	25						
		High/No	24						
		High/Yes	12						
335	GBM Pattern (Corr.)	Low	34	3.0×10^{-5}	Univariate	2.4	1.6– 3.6	4.9×10^{-5}	0.72
		High	14						
	TCGA Karnofsky Score	≥60	15	1.0×10^{-5}		4.1	2.1– 8.1	4.7×10^{-5}	0.81
		<60	5						
	GBM Pattern (Corr.)	Low/≥60	34	1.6×10^{-8}	Bivariate	2.3	1.5– 3.5	6.9×10^{-5}	0.74
	TCGA Karnofsky Score	High/≥60	15			3.8	1.9– 7.6	1.1×10^{-4}	
		High/<60	5						

Table S4 (captions on p. S12).